Available online at www.sciencedirect.com
SCIENCE DIRECT®
Chemical Physics Letters 376 (2003) 1–5
CHEMICAL PHYSICS LETTERS
www.elsevier.com/locate/cplett

Size-dependent electronic transition rates in cubic nanocrystalline europium doped yttria

Hongwei Song *, Jiwei Wang, Baojiu Chen, Hongshang Peng, Shaozhe Lu

Key Laboratory of Excited State Physics, Institute of Optics, Fine Mechanics and Physics, Chinese Academy of Sciences, 140-Ren-Min Street, Changchun 130022, PR China

Received 7 January 2003; in final form 11 May 2003
Published online: 27 June 2003

Abstract

In cubic nanocrystalline as well as polycrystalline Y_2O_3:Eu^{3+} prepared by combustion, the radiative transition rate of $^5D_1$–$^7F_1$ and the nonradiative relaxation rate of $^5D_1$–$^5D_0$ were obtained by measuring the temperature-dependence of emission intensity and lifetime. The results indicate that the radiative and nonradiative rates both increase with decreasing particle size. The increase of radiative transition rate was attributed to the lower symmetry surrounding the Eu^{3+} ions, while the increase of nonradiative relaxation rate to the additional nonradiative relaxation channels caused by surface defects.

1. Introduction

Rare earths in insulating nanoparticles are attracting interest currently because of their potential application in luminescence and display. The scientific understanding of modified electronic and optical properties in insulating nanoparticles is also significant from the fundamental point of view [1–8]. Among rare earth doped nanoparticles, nanocrystalline europium doped yttria, Y_2O_3:Eu is a typical one, because polycrystalline Y_2O_3:Eu is the main and unsurpassed red emitting material in fluorescent lamps and projection television tubes. It is expected that the luminescent efficiency and the resolution of display be enhanced in nanosized particles. Much work has been performed on the electronic and optical properties of Y_2O_3:Eu during the last few years [9–14]. R.S. Meltzer and his co-workers studied the electron–photon interaction by persistent spectral hole burning. They also observed that the radiative lifetime in nanocrystalline Y_2O_3:Eu^{3+} depended on the surrounding medium [7,11]. Igarashi et al. [6] reported that the lattice distortion of nanoparticles was much larger than that of the polycrystals. Wakefield et al. reported that the quantum efficiency of cathodoluminescence in nanocrystalline Y_2O_3:Eu was higher than that in polycrystalline Y_2O_3:Eu. In a previous paper, we observed ultraviolet light-induced intensity change in the charge transfer band [5].

* Corresponding author. Fax: 864316176320.
E-mail address: songhongwei2000@sina.com.cn (H. Song).

0009-2614/03/$ - see front matter © 2003 Elsevier Science B.V. All rights reserved.
doi:10.1016/S0009-2614(03)00810-8

For real applications, one of the most significant tasks is to improve the quantum efficiency of photoluminescence in nanoparticles. However, there has been no breakthrough in this field until now. Studying electronic transition processes is helpful to solve this problem. In this Letter, to analyze the radiative and nonradiative transition processes, the temperature-dependent luminescent characteristic of the $^5D_1$–^7F_J transitions in nanocrystalline Y_2O_3:Eu prepared by combustion were studied. It should be pointed out that, Meltzer has worked on the transition processes of $^5D_0$–^7F_J in monoclinic yttria, whereas Wakefield has reported results in cubic yttria [4,7].

2. Experiments

Two kinds of nanocrystalline Y_2O_3: Eu^{3+} (1% in molar ratio) powders were prepared by combustion. The polycrystalline powders were obtained by annealing at 1200 °C. The sample preparations were given in one of our previous paper [5]. All the powders were cubic in symmetry, which was confirmed by X-ray diffraction (XRD). In the light of the Scherrer formula, the sizes of the two kinds of nanoparticles were determined to be ~5 and ~20 nm, respectively. This was also confirmed by a survey of transition electronic microscopy graph (TEM, see Fig. 1). The average size of the polycrystalline powders was ~3 μm. Most of time, the samples were stored in a black bottle under inert atmosphere.

A 266-nm light was used for excitation, with a line width of 1 cm^{-1}, repetition frequency of 10 Hz and pulse duration of 10 ns. It was generated from a Nd:YAG laser combined with a Fourth-Harmonic-Generator. For measurement, the powder samples were put into a liquid-helium-cycling-system, in which the temperature varied from 10 to 300 K. The spectra were recorded by a Spex 1403 spectrometer, a photomultiplier, a boxcar averager and computer data acquisition.

3. Results and discussion

$^5D_1$ is an intermediate excited state among ^5D_J ($J = 0, 1, 2$), thus it is suitable to study the non-

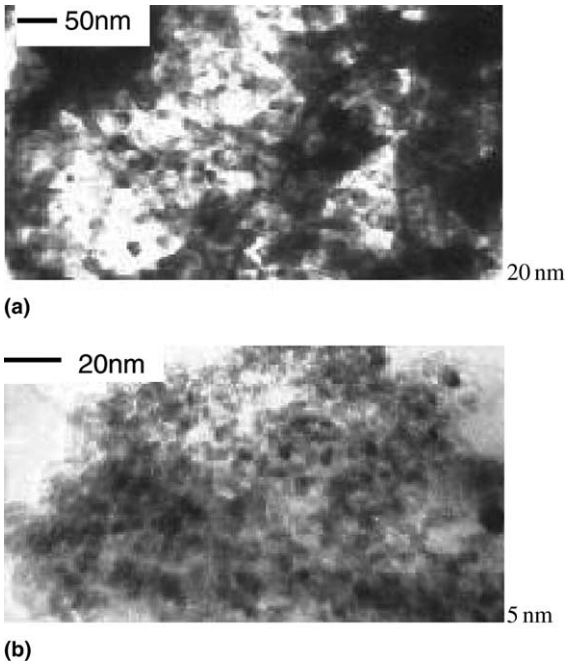

Fig. 1. Transition electronic micrograph of the cubic nanocrystalline Y_2O_3:Eu^{3+}.

radiative relaxation processes occurring among ^5D_J. Fig. 2 shows the emissions of $^5D_1$–$^7F_1$ in different Y_2O_3:Eu powders. There are three groups of lines, in the range of 18 500–18 650, 18 650–18 800 and 18 850–19 000 cm^{-1}, respectively. Each group has two lines (The two lines in the range of

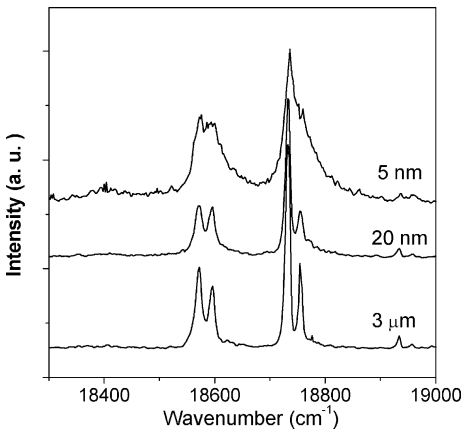

Fig. 2. Emission spectra of the $^5D_1$–$^7F_1$ transitions in various nanocrystalline Y_2O_3:Eu^{3+} at 10 K. (In the measurement, the delay time is 10 μs.)

18 850–19 000 cm^{-1} are quite weak). In cubic Y_2O_3:Eu, the $^5D_1$ and $^7F_1$ levels both split into three lines according to Stark effect. The energy separation between two neighboring components of $^5D_1$ is several ten wavenumbers, while that of $^7F_1$ is more than one hundred wavenumbers [15]. At 10 K, only the two lowest Stark components of $^5D_1$ are populated considering the energy separation. In Fig. 2, the three groups were associated with the three crystal-field components of $^7F_1$ and the two lines in each group with the two lowest crystal-field components of $^5D_1$. It can be also seen that the smaller the particle size, the wider the full line width. Fig. 3 shows the emission intensity of the $^5D_1$–$^7F_1$ transitions as a function of temperature. It was seen that the emission intensity decreased with increasing temperature. The intensity decreased more rapidly in nanocrystalline Y_2O_3:Eu, indicating that the temperature quenching effect became stronger. In 1970, Fonger and Struck systemically studied the temperature-quenching effect of Eu^{3+}. According to their results, two paths, the ^5D quenching via two-step ^5D–CTS–^5D and the quenching via one step ^5D_J–$^5D_{J-1}$, contribute to the temperature quenching of Eu^{3+} [16,17].

Fig. 4 shows the fluorescence decay curves of $^5D_1$–$^7F_1$ measured at 10 K. It was seen that the $^5D_1$–$^7F_1$ transition decayed exponentially in the studied time scale. The smaller the particle size was, the faster the decay was. Under 266-nm excitation, electrons were excited from ground states to CTS firstly, and then were feed to excited ^5D_J states. The population of $^5D_1$ came from the nonradiative CTS feeding and the $^5D_2$–$^5D_1$ relaxation. The CTS feeding of ^5D is faster than the decay of ^5D. The radiative $^5D_1$–^7F_J transitions, one-step nonradiative $^5D_1$–$^5D_0$ relaxation and two-step nonradiative $^5D_1$–CTS–^5D_J relaxation contributed to the depopulation of $^5D_1$. In Y_2O_3:Eu, the lifetime had only a little variation as the concentration of Eu^{3+} was less than 1 % (in molar ratio), thus the cross relaxation among Eu^{3+} ions was neglected.

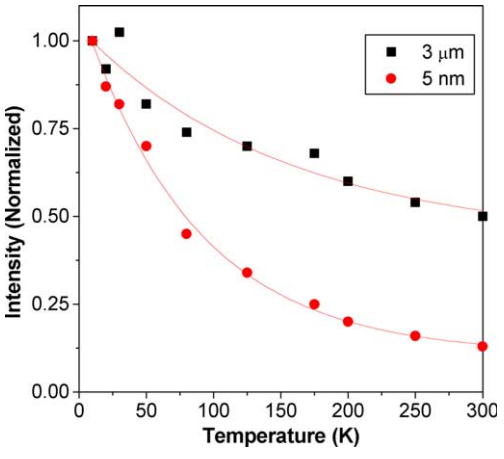

Fig. 3. Dependence of the integral intensity of the $^5D_1$–$^7F_1$ transition on temperature. The integral intensity of $^5D_1$–$^7F_1$ at 10 K for each sample was normalized.

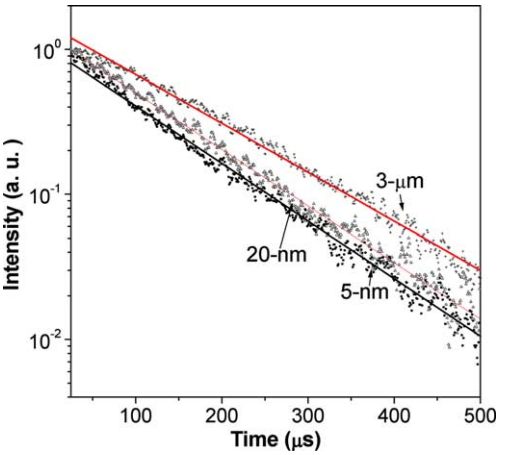

Fig. 4. Fluorescent decay curves of the $^5D_1$–$^7F_1$ transitions at 18 735 cm^{-1} in various Y_2O_3:Eu^{3+} powders.

To obtain the nonradiative relaxation and radiative transition rates, we measured the dependence of the $^5D_1$–$^7F_1$ lifetime on temperature, which was drawn in Fig. 5. The lifetime of $^5D_1$–$^7F_1$ remained as a constant below 100 K, and decreased with increasing temperature above 100 K. As is well known, the reverse of lifetime equals to the sum of the radiative transition and nonradiative relaxation rates. The lifetime of $^5D_1$ can be written as,

$$\tau_1(T) = \frac{1}{W_1 + W_{10}(T)}, \quad (1)$$

where W_1 is the radiative transition rate of $^5D_1$–$\sum_J {}^7F_J$ and W_{10} is the nonradiative relaxation rate

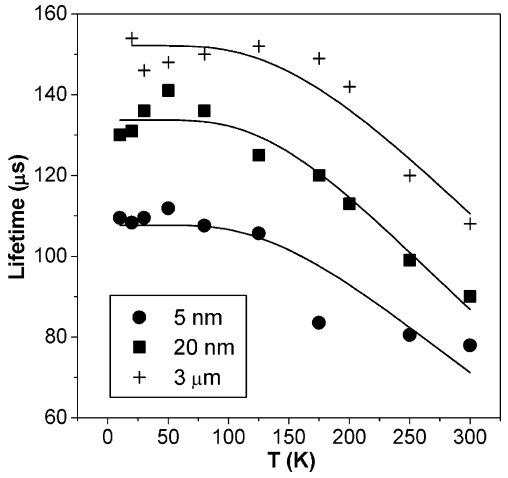

Fig. 5. Dependence of fluorescent lifetime of $^5D_1$–$^7F_1$ on temperature. The dots are experimental data and the solid curves are fitting functions.

of $^5D_1$–$^5D_0$. Here, we have neglected the two-step nonradiative $^5D_1$–CTS–^5D relaxation for simplicity. In the light of the theory of multi-phonon relaxation, W_{10} can be written as,

$$W_{10}(T) = W_{10}(0)[1+ < n >]^{\Delta E_{10}/\hbar\omega}, \quad (2)$$

where $W_{10}(0)$ is the nonradiative relaxation rate at 0 K, ΔE_{10} is the average energy separation from $^5D_1$ to $^5D_0$, $\hbar\omega$ is the phonon energy, k is Boltzmann's constant and $\langle n\rangle = 1/(e^{\hbar\omega/kT} - 1)$ is the phonon density. According to Eqs. (1) and (2), we have

$$\tau_1 = \frac{1}{W_1 + W_{10}(0)[1 - e^{-\hbar\omega/kT}]^{-\Delta E_{10}/\hbar\omega}}. \quad (3)$$

We well fitted the dependence of $^5D_1$ lifetime on temperature in different Y_2O_3:Eu powders, as shown in Fig. 5. In the fitting, we chose $\Delta E_{10} = 1540\ cm^{-1}$, $\hbar\omega = 377\ cm^{-1}$. Actually, we measured the Raman scattering spectra of the powder samples and observed that the 377 cm^{-1} vibration mode was dominant in polycrystalline Y_2O_3. It became broader as the particle size decreased to several ten nanometers. It is well known that Y_2O_3 absorbs CO_2 and H_2O from the atmosphere, and it has been shown that nanosized Y_2O_3 samples are especially prone to this behavior, due to the high surface area [18,19]. We observed the vibration associated to carbonate groups by Raman scattering spectra [19]. In comparison to the 377 cm^{-1} mode, the vibration caused by carbonate groups is weaker, even in nanocrystalline Y_2O_3. In addition, we also fitted the experimental dots in Fig. 5 taking $\hbar\omega$ as a variable parameter. The results indicate that the 377 cm^{-1} vibration mode dominantly contributes to the nonradiative relaxation of $^5D_1$–$^5D_0$. Despite of this, we can not conclude that the adsorption of CO_2 has no influence on nonradiative relaxation of $^5D_1$–$^5D_0$. Further work should be performed on studying the relationship between nonradiative relaxation and the contamination.

W_1 and W_{10} were obtained by fitting, which were listed in Table 1. It appears that the radiative and nonradiative rates both increase with decreasing particle size. In rare earth ions, the diameter of electronic wavefunctions of f states is in the order of 10^{-1} nm, which is much smaller than the particle size. In this case, the quantum size effect does not work. The increase of radiative transition rate with decreasing particle size was attributed to the lower local symmetry surrounding Eu^{3+}. In nanoparticles, more atoms are located in/near the particle surface, and numerous surface defects exist. These defects may increase the degree of disorder and lower the local symmetry of Eu^{3+} ions located in/near the surface of the particles. As a consequence, the radiative transition rate of $^5D_1$–^7F_J increases. As is well known, the $^5D_0$–$^7F_2$ transition is electric dipole transition and the $^5D_0$–$^7F_1$ transition is a magnetic dipole one. The intensity ratio of $^5D_0$–$^7F_2$ to $^5D_0$–$^7F_1$ depends strongly on the local symmetry surrounding the Eu^{3+} activators. The increased intensity ratio of $^5D_0$–$^7F_2$ to $^5D_0$–$^7F_1$ points toward a lower local symmetry surrounding Eu^{3+}. By emission spectra, the intensity ratios in the 5-nm, 20-nm and the 3-μm powders were deter-

Table 1
Variation of radiative transition and nonradiative relaxation rates with particle size

Particle size	5-nm	20-nm	3-μm
W_1 (ms^{-1})	4.7	4.1	3.8
$W_{10}(0)$ (ms^{-1})	4.5	3.2	2.7

mined to be 5.2, 4.2 and 3.8, respectively [20]. This indicates that the local symmetry surrounding Eu^{3+} ions decreases indeed. One possible reason for the lower symmetry in nanoparticles is that the adsorption of CO_2/H_2O creates a local distortion on some of the sites accommodating Eu^{3+} ions. As to the increase of nonradiative relaxation with decreasing particle size, can be also attributed to surface effects. The surface defects take as nonradiative transition channels, leading the nonradiative relaxation rates to increase with decreasing particle size.

4. Conclusions

In nanocrystalline Y_2O_3:Eu, due to the existent of numerous surface defects, the local symmetry surrounding Eu^{3+} became lower, causing the electric dipole transition rate of $^5D_1$–$^7F_1$ to increase. At the same time, the nonradiative relaxation rate also increased due to the surface defects acted as nonradiative transition channels. These two facts lead the lifetime of $^5D_1$ to decrease with decreasing particle size.

Acknowledgements

This work was supported by One Hundred Talents Project, sponsored by Chinese Academy of Sciences.

References

[1] W. Chen, J. Malm, Y. Huang, S. Liu, R. Wallenberg, J. Bovin, Phys. Rev. B 61 (2000) 11021.
[2] S. Qu, W. Zhou, F. Liu, N. Chen, Z. Wang, Appl. Phys. Lett. 80 (2002) 3605.
[3] Z. Wei, L. Sun, C. Liao, C. Yan, Appl. Phys. Lett. 80 (2002) 1447.
[4] G. Wakefield, E. Holland, P.J. Dobson, Adv. Mater. 13 (2001) 1557.
[5] H. Song, B. Chen, H. Peng, J. Zhang, Appl. Phys. Lett. 81 (2002) 1776.
[6] T. Igarashi, M. Ihara, T. Kusunoki, K. Ohno, Appl. Phys. Lett. 76 (2000) 1549.
[7] R.S. Melzer, K.S. Hong, Phys. Rev. B 61 (2000) 3396.
[8] J. Dhanaraj, R. Jagannathan, T. Kutty, C. Lu, J. Phys. Chem. B 105 (2001) 11098.
[9] G. Blasse, B.C. Grabmaier, Luminescent Materials, Springer, Berlin, 1994.
[10] Y. Tao, G. Zhao, W. Zhang, S. Xia, Mater. Res. Bull. 32 (1997) 501.
[11] R.S. Meltzer, S.P. Feofilov, B. Tissue, H.B. Yuan, Phys. Rev. B 60 (1999) 14012.
[12] A. Konrad, T. Fries, A. Gahn, F. Kummer, J. Appl. Phys. 86 (1999) 3129.
[13] D.K. Williams, H. Yuan, B.M. Tissue, J. Lumin. 83–84 (1999) 297.
[14] R. Schmechel, M. Kennedy, H.V. Seggern, J. Appl. Phys. 89 (2001) 1679.
[15] J. Heber, K.H. Hellwege, U. Kuler, H. Murmann, Z. Phys. (1970) 189.
[16] C.W. Struck, W.H. Fonger, Phys. Rev. B 4 (1971) 22.
[17] W.H. Fonger, C.W. Struck, J. Chem. Phys. 52 (1970) 6364.
[18] J.A. Capobianco, F. Vetrone, T.D. Alesio, A. Speghini, M. Bettinelli, Phy. Chem., Chem. Phys. 2 (2002) 3203.
[19] J.A. Capobianco, F. Vetrone, J.C. Boyer, A. Speghini, M. Bettinelli, J. Chem. Phys. B 106 (2002) 1181.
[20] H. Song, B. Chen, B. Sun, J. Zhang, S. Lu, Chem. Phys. Lett. 372 (2003) 368.